Paper:
Almatani, T., Hugtenburg, R., Lewis, R., Barley, S. & Edwards, M. (2016). Automated algorithm for CBCT-based dose calculations of prostate radiotherapy with bilateral hip prostheses. *The British Journal of Radiology, 89*(1066), 20160443
http://dx.doi.org/10.1259/bjr.20160443

Automated algorithm for CBCT-based dose calculations of prostate radiotherapy with bilateral hip prostheses

Turki Almatani[1,2*], Richard P. Hugtenburg[1,3], Ryan D. Lewis[3], Susan E. Barley[4], and Mark A. Edwards[3]

[1]College of Medicine, Swansea University, Singleton Park, Swansea SA2 8PP, UK
[2]Umm Al-Qura University, Makkah, KSA
[3]Department of Medical Physics and Clinical Engineering, Singleton Hospital, ABM University Health Board, Swansea SA2 8QA, UK
[4]Oncology Systems Limited, 14 Longbow Close, Shrewsbury SY1 3GZ, UK

[*]Corresponding author. E-mail address: turkialmatani@gmail.com (T. Almatani)

Objective: Cone beam CT (CBCT) images contain more scatter than a conventional CT image and therefore provide inaccurate Hounsfield units (HU). Consequently CBCT images cannot be used directly for radiotherapy dose calculation. The aim of this study is to enable dose calculations to be performed with the use of cone-beam CT images taken during radiotherapy and evaluate the necessity of re-planning.

Methodology: A prostate cancer patient with bilateral metallic prosthetic hip replacements was imaged using both CT and CBCT. The multilevel threshold algorithm (MLT) was used to categorise pixel values in the CBCT images into segments of homogeneous HU. The variation in HU with position in the CBCT images was taken into consideration. This segmentation method relies upon the operator dividing the CBCT data into a set of volumes where the variation in the relationship between pixel values and HUs is small. An automated MLT algorithm was developed to reduce the operator time associated with the process. An intensity modulated radiation therapy (IMRT) plan was generated from CT images of the patient. The plan was then copied to the segmented CBCT data sets with identical settings and the doses were recalculated and compared.

Results: Gamma evaluation showed that the percentage of points in rectum with $\gamma < 1$ (3%/3 mm) were 98.7% and 97.7% in the segmented CBCT using MLT and the automated MLT algorithms, respectively. Compared with the planning CT (pCT) plan, the MLT algorithm showed -0.46% dose difference with 8 hours operator time while the automated MLT algorithm showed -1.3%, which are both considered to be clinically acceptable, when using collapsed cone (CC) algorithm.

Conclusion: The segmentation of CBCT images using the method in this study can be used

for dose calculation. For a prostate patient with bilateral hip prostheses and the associated issues with CT imaging, the MLT algorithms achieved a sufficient dose calculation accuracy that is clinically acceptable. The automated MLT algorithm reduced the operator time associated with implementing the MLT algorithm to achieve clinically acceptable accuracy. This saved time makes the automated MLT algorithm superior and easier to implement in the clinical setting.

Advance in knowledge: The MLT algorithm has been extended to the complex example of a patient with bilateral hip prostheses, which with the introduction of automation is feasible for use in ART, as an alternative to obtaining a new planning CT and re-outlining the structures.

1 Introduction

One of the desirable objectives during external beam radiotherapy (EBRT) of the prostate is the delivery of an uniform radiation dose to the treatment volume while sparing organs at risk. In practice, this may be difficult to achieve due to day-to-day changes in patient positioning, patient shape and internal organ movement during the treatment course (1). Interfractional motions such as variations in bladder and rectum volume have been demonstrated to have significant effects on prostate position and a negative impact on the accuracy of the treatment course (2).

The implementation of image guided radiation therapy (IGRT) in clinical practice, such as kilovoltage cone beam computed tomography (kV-CBCT), has improved tumor targeting and tumour control during the treatment delivery process and reducing dose delivery to normal tissues. CBCT has been used to correct patient set-up in the treatment position and to monitor any anatomical deformations in 3D with sufficient soft tissue contrast (3). In addition, CBCT can be feasible for adaptive radiotherapy (ART), e.g. dose recalculation, if the Hounsfield units (HU) are accurate and reliable (4).

Due to its cone-beam geometry, the amount of scatter in CBCT images is greater than that of conventional CT images (fan beam),and is dependent on the scanned object size, the collimator and the filter used (5). The image quality also depends on acquisition parameters, i.e. mA, kV and the number of projections. In addition, limited gantry rotation speed and large field-of-view (FOV) in a single rotation reduce image quality. Therefore, CBCT images provide inaccurate HUs and, consequently, cannot be used directly for dose calculation (6). Therefore, if there are significant anatomical changes observed on the

CBCT images, acquiring another CT is necessary for an accurate assessment of dose differences. This procedure is time consuming across all staff groups involved in the radiotherapy pathway and additional dose is delivered to the patients. Thus it would be sufficient to use CBCT images that were already taken during radiotherapy for evaluating the necessity of re-planning. Many papers have studied the use of CBCT data for dose recalculation, which is still an active area for research (6).

To deal with HU calibration of CBCT images, Richter et al (2008) proposed a method where HU-electron density conversion curves were based on average CBCT HU values for separate treatment sites in order to generate population-specific conversion curves (7). Such an approach is still subject to CBCT artefacts and can result in dose calculation errors of greater than 5% when compared to planning CT (pCT) -based dose calculation (6). Some studies deal with correcting scatter by applying quite unsophisticated software corrections to CBCT images before reconstruction (8). Such a method may be unable to accurately reconstruct higher-density material for a large scanned object size. In addition, it may be difficult to implement such a method in a clinic even though recent commercial software releases provide sophisticated scatter correction algorithms (9).

Other studies deal with adjustment techniques to correct CBCT HU values, such as mapping the HUs in CT images to the equivalent points in the CBCT image geometry after rigid or deformable image registration (10, 11). In addition, image cumulative histograms can be used to adjust HU values between pCT and CBCT images (10, 14). Another technique uses a multilevel threshold (MLT) algorithm as proposed by Boggula et al (2007), where the pixel values of CBCT images were replaced with a small number of fixed HU values as in CT for air, soft tissue and bone (12-14). Onozato et al (2014) excluded

129 water and used fat and muscle instead, resulting in a dosimetric difference below 2% (14).
130 In addition, Fotina et al (2008) used the same technique, calling it a density override
131 technique, but with a range of HU values for bone (soft bony structures, hard bone and
132 teeth) and air/low density regions (rectal balloon and lung). All other regions are assumed
133 to be water-equivalent assigned with one HU value, resulting in a dosimetric difference
134 below 2% (6).

135 Recently, Dunlop et al (2015) assessed the CBCT dose calculation accuracy for density
136 override approaches for four pelvis cases, where CBCT voxels were assigned as water only
137 and then as either water or bone (water only and water-and-bone methods). This was then
138 compared with a scatter correction and automated density override approach that is
139 available in the RayStation TPS (V3.99, RaySearch Laboratories, Stockholm, Sweden) (9).
140 In the automated density override approach, six different densities (air, lung, adipose tissue,
141 connective tissue, cartilage/bone, and higher density for prosthesis) are assigned to the
142 CBCT image by binning the CBCT image histogram into six density levels. Compared
143 with pCT acquired on the same day as the CBCT, the results showed that the automated
144 approach was superior to the other methods, when considering smaller patients (with
145 anterior-posterior distance < 25 cm). For larger patients, the water only method gave the
146 best accuracy.

147 The occurrence of inhomgeneities in the patient anatomy, e.g. hip replacements, has the
148 ability to complicate the automated process, requiring the addition of additional set
149 densities. In fact, none of the above studies used a patient with prostheses, which would
150 provide a more general assessment of dose calculation using CBCT. Almatani et al (2016)
151 studied CBCT-based dose calculations of a prostate patient with a single hip prosthesis

using the MLT algorithm. The work showed that it was necessary to extend the MLT algorithm to categorise pixel values into segments on a region-by-region basis, with the region size changing depending on the anatomical features (15). In addition, a larger number of materials (up to 8) than typically used in previous works was explored. The results showed that five values of HU (air, adipose, water, cartilage/bone and metal implant) gave the best balance between dose accuracy (–1.9%) and operator time (3.5 hours). However, the length of operator time needed could make it difficult to implement this as a technique in the clinic.

The aim of this work is to develop a more robust method to account for the full range of patient size as well as the difficulties presented by the metal artefacts in both pCT and CBCT images. A CBCT-based dose calculation of a patient with bilateral metal hip prostheses is presented using the extended MLT algorithm, in the same manner extending upon proposed previously by the authors for a single hip prosthesis. In addition, an automated MLT algorithm was developed to reduce the operator time associated with the manual MLT algorithm. With the flexibility of a region-by-region approach, it is envisaged that the method can be applicable for the automation of dose calculation on segmented magnetic resonance (MR) images and could be of interest to MR-based ART (9).

2 Method and materials

2.1 CBCT image acquisition

The X-ray volumetric imaging integrated in an Elekta Synergy linear accelerator (XVI^{TM}, version 4.5, Elekta, Crawley, West Sussex, UK) was used to acquire CBCT images. The CBCT scans were acquired with a field of view (medium FOV) of 41 cm in diameter and

17.85 cm in the axial direction with a bowtie filter added (F1). CBCT images were reconstructed with 1 mm cubic voxels and averaged in the longitudinal direction for 3 mm slice thickness. The images were then transferred to the Oncentra MasterPlan (OMP) treatment planning system (version 4.3 Elekta, Netherlands) via DICOM protocol for dose calculation.

2.2 Patient study

This study was performed on a patient with bilateral metal hip prostheses replacement treated at the Department of Clinical Oncology and Radiotherapy, South West Wales Cancer Centre ABM University Health Board, Swansea, Wales. The anterior-posterior (AP) separation of the patient was 26.5 cm. Such a challenging case provides a good assessment of dose calculation using CBCT due to the difficulties presented by the metals artefacts in both pCT and CBCT images. The artefacts in pCT were reassigned as water in the original patient plan using a bulk density correction (Fig. 1a). An intensity modulated radiotherapy (IMRT) treatment with five 6-MV photon fields, at gantry angles of 35°, 145°, 180°, 235°, and 300° was performed. The prescription dose was 70 Gy in 35 fractions. Dose distribution was calculated using pencil beam (PB) and collapsed cone (CC) algorithms to allow the comparison with Monte Carlo (MC) algorithm and to identify the effects of HU on dose calculation.

2.3 Modification of CBCT images

The MLT algorithm, used to correct CBCT data, involves categorising pixel values in the CBCT images into segments of homogeneous HU using MATLAB scripts (Mathworks,

195 Natick, MA) to generate segmented CBCT (sCBCT) data. Based on Almatani et al (2016),
196 the binning of CBCT images of a patient with hip prosthesis into five HU values results in
197 sufficiently accurate and clinically acceptable dose distribution (15). Considering more
198 than five HU values provides more anatomical information and improves dose calculation
199 accuracy (by 0.23%) but would require more operator time (58%), as the sensitivity
200 increases when increasing the number of HU bins to define the material type. Therefore, in
201 this study, five values of HU values were used to segment CBCT images that represent, air
202 (–976 HU), adipose tissue (– 96 HU), water (0 HU), 2/3 cartilage & 1/3 bone (528 HU)
203 and metal implants (2976 HU). The ranges of pixel values in the CBCT images were: air
204 (0 to 200), adipose tissue (201 to 700), water (701 to 875), 2/3 cartilage & 1/3 bone (876
205 to 1600) and metal implant (1601 to 8000).

206 The threshold values for each material at these intervals are dependent on the geometry
207 since noise and scatter in CBCT is variable, especially in the presence of high density
208 materials, as shown in Figure 1(b) (16). In this study, the MLT algorithm was used in two
209 ways, using a manual and an automated procedure. In the manual procedure, the CBCT
210 images were divided into regions with sets of different threshold values, which are
211 determined on a region-by-region basis, to sufficiently correct for the artefacts. The shape
212 of each region is a rectangular cuboid. In general, the greater the variation in the scatter,
213 the greater the number of regions that need to be considered, and the size of the region
214 decreases as it gets closer to inhomogeneities. The resultant segmented CBCT images using
215 this procedure are referred to as $sCBCT_{man}$.

In the automated procedure, the CBCT images were divided into five concentric rings, which are uniform in shape through all slices, using MATLAB scripts, as shown in Figure 1(d). The centre of the inner radius (radius 1) was defined at the centre of the patient geometry, which can be changed by the user. The lower threshold values for each material changes with the radius but is easily determined by the user's analysis of the central slice. For example, the lower threshold value for water, in the inner radius, was defined in relation to the pixel value with the maximum frequency in the slice according to the ratio of the lower threshold value of water and the pixel value with the maximum frequency in the central slice. The same procedure was applied for each material in each radius. The resultant segmented CBCT images using this procedure are referred to as $sCBCT_{auto}$.

The use of a radial shape was motivated by the fact that, in CBCT, the issue of the scatter

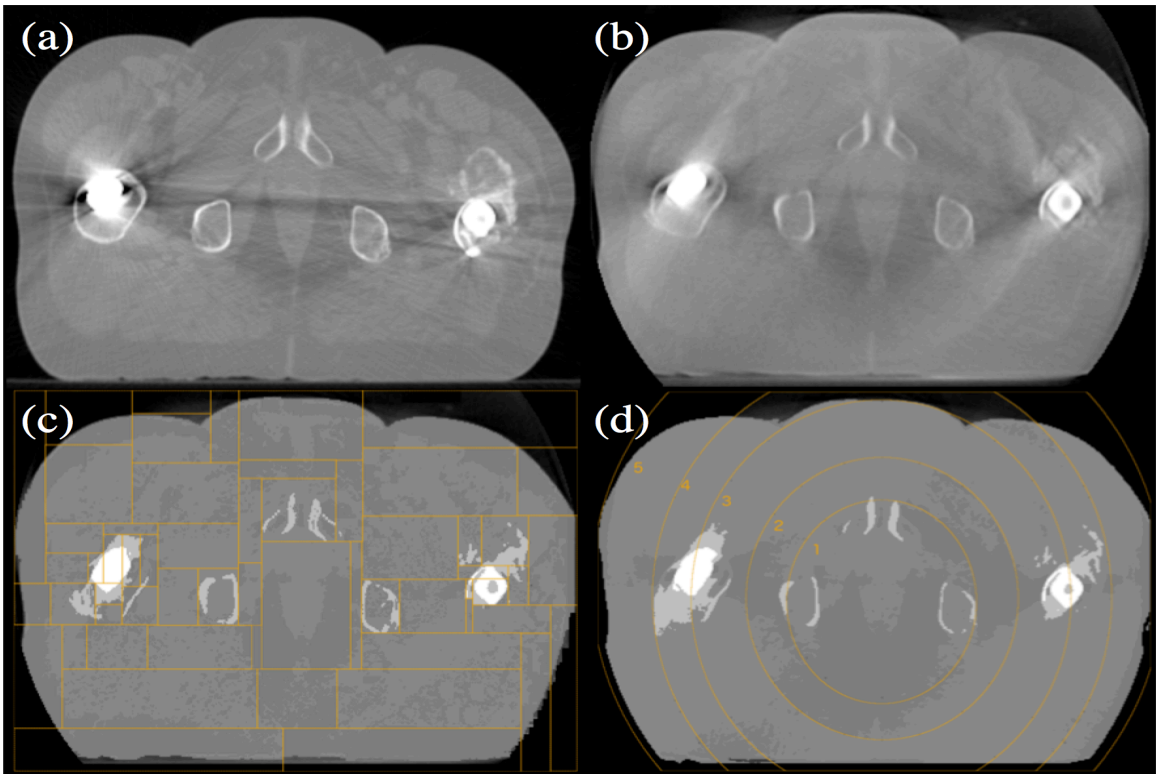

Figure 1: A slice of the pCT (a) and the original CBCT (b) and the resultant images after segmentation CBCT using the manual MLT ($sCBCT_{man}$) and the automated MLT ($sCBCT_{auto}$) (c and d respectively).

occurs spherically and ring artefacts that caused by miscalibrated detector pixel lines/rows, elements or manufacturing defects at a fixed location in the flat panel detector (FPD). In addition, due to the presence of the bilateral hip, the low energetic X-rays are absorbed, thus the polychromatic beam becomes gradually harder. Consequently, the FPD exhibits pixel-to-pixel sensitivity variations, that lead to ring artefacts (17). In a pelvic region with prostheses, there is a rapid change in the exposure to the FPD from frame to frame, receiving high exposure then followed by low exposure due the strong attenuation of the metal. This leads to so-called radar artefacts that appear as a circular radar bright-shaded region, owing to inconsistencies in detector signal and/or gain (18).

2.4 Monte Carlo calculation

The Elekta Synergy linear accelerator was modeled using Electron Gamma Shower (EGSnrc), which is one of the most popular MC codes for medical physics (19). BEAMnrc and DOSXYZnrc are two applications in EGSnrc code that are used to simulate the beam generated from the treatment head and to score dose deposition in voxel grids, respectively. In this study, 90 million particles were used for each beam to provide an accurate simulation with a low statistical uncertainty. High performance computing (HPC-Wales) was used to speed up MC calculations (20). The MC normalization was performed by calculating the dose in a water phantom under the standard reference conditions (10 ×10 field size, 100 cm source-to-surface distance, 5 cm depth).

2.5 Treatment planning evaluation and comparison

The sCBCT (both $sCBCT_{man}$, $sCBCT_{auto}$) and pCT images fusion was accomplished with

manual rigid registration using ProSoma software (v3.3, MedCom, Germany) and the structure sets were then transferred to the sCBCT images without any modification except the external contour. The plans were then copied to sCBCT using the same geometry and MU values and doses were recalculated using PB and CC algorithms. For MC calculation, the pCT artefacts, caused by the presence of the hip prostheses, were changed to a water material of uniform density using a MATLAB script. The MC dose calculation was then performed on pCT and sCBCT images using the same HU-ED calibration as in OMP. The MC dose file (.3ddose) and the DICOM-RT file were then imported into the computational environment for radiotherapy research (CERR) software to compare the resultant dose distribution (21). Dose volume histograms (DVH) were compared between pCT and sCBCT plans. The maximum dose (D_{max}), mean dose (D_{mean}) and minimum dose (D_{min}) parameters for PTV (prostate and seminal vesicles), rectum and bladder were compared. The coverage of the PTV, the dose to 95% of the PTV (D95%) and the relative volume doses delivered to the rectum and bladder (V65 and V70) were compared. In addition, the volume of right/left hip and bone were calculated in the pCT scan and compared with those in the $sCBCT_{man}$ and $sCBCT_{auto}$ scan to show how close the two scans were. To quantitatively appraise the differences between pCT and sCBCT plans, especially for the PTV, rectum and bladder, a gamma index analysis was performed using the pCT plan as a reference. The criteria were set as 3 mm distance to agreement (DTA) and 3% dose difference (DD) and 5% low dose threshold. The conformity index (CI) was calculated for all sCBCT plans and then compared with the pCT plans using PB, CC and MC algorithms (22). In addition, the dose at the isocentre (at the geometric centre of the prostate PTV (PTVp)) was compared between the pCT and $sCBCT_{man}$ and $sCBCT_{auto}$ plans.

3 Results and discussion

Figure 2 shows the cross-plane profile/x profile of pCT, $sCBCT_{man}$ and $sCBCT_{auto}$ at the depth of the plan isocentre as well as the CT number of the pCT, $sCBCT_{man}$ and $sCBCT_{auto}$ scans at that depth. In general, the $sCBCT_{man}$ and $sCBCT_{auto}$ profiles are in good agreement with the pCT profile especially at the implant/tissue interface. For bone regions, the $sCBCT_{auto}$ numbers showed less agreement with pCT numbers, compared with $sCBCT_{man}$ numbers where some of these regions were considered as water. In addition, the $sCBCT_{auto}$ overestimated some adipose tissue regions and considered it as water, especially in the PTV region (high-dose region), leading to an underestimation of the dose in that region by –4.4%. On the other hand, $sCBCT_{man}$ numbers considered more adipose tissue

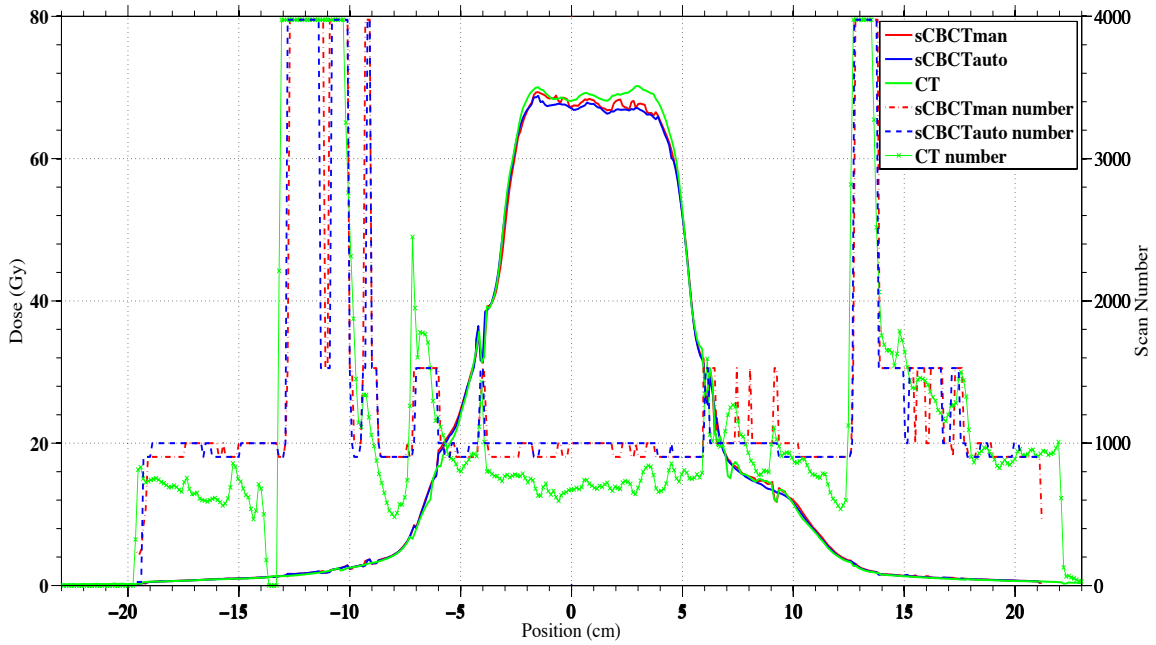

Figure 2: Comparison of the dose profile of pCT, $sCBCT_{man}$ and $sCBCT_{auto}$ plans at the isocentre depth using MC algorithm. The second y axis represents the $sCBCT_{man}$ number, $sCBCT_{auto}$ number and CT number.

than $sCBCT_{auto}$ numbers, thus the dose difference with the pCT dose profile was less when compared with the $sCBCT_{auto}$ dose profile. The largest difference between the pCT and

sCBCT$_{man}$ and sCBCT$_{auto}$ plans was in the PTV region where pCT was 69.1 Gy, sCBCT$_{man}$ was 66.1 Gy and sCBCT$_{auto}$ was 65.8 Gy when using MC algorithm.

Figure 3 shows the differences in the right (RT)/left (LT) hip and bone volumes between the pCT scan, sCBCT$_{man}$ and sCBCT$_{auto}$ scans. Compared with the pCT scan, the largest difference between sCBCT$_{man}$ and sCBCT$_{auto}$ was found in the LT hip where in sCBCT$_{man}$ it was overestimated by 6.8% and underestimated by –30.2% in sCBCT$_{auto}$. This underestimation was due to the fact that the automated MLT algorithm was unable to accurately correct cupping artefacts due to the increased amount of scatter and beam hardening inside the LT hip, resulting in dark streaks (17, 18). Thus, the automated MLT algorithm erroneously replaced the artefacts with bone HU values while the manual MLT correctly replaced the artefacts with metal HU values as shown in Figure (4). On the other hand, both MLT algorithms overestimated the RT hip where scatter and bright streak

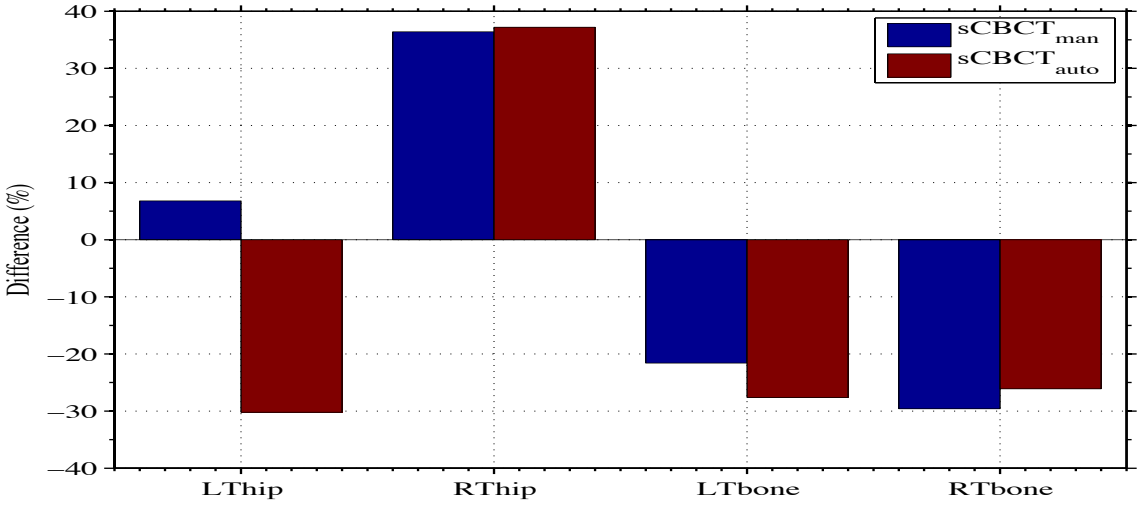

Figure 3: Right/Left hip and bone volume differences between pCT and sCBCT$_{man}$/sCBCT$_{auto}$.

artefacts were erroneously replaced with hip HU values, leading to a significant reduction in the RT bone volume around that region. Another reason for the underestimation of both

297 bone volumes in both MLT algorithms might be due to the fact that streak artefacts in pCT
298 increased the number of high HU values and were not corrected (only for dose calculation),
299 where in sCBCT, both MLT algorithms attempted to correct for this.
300

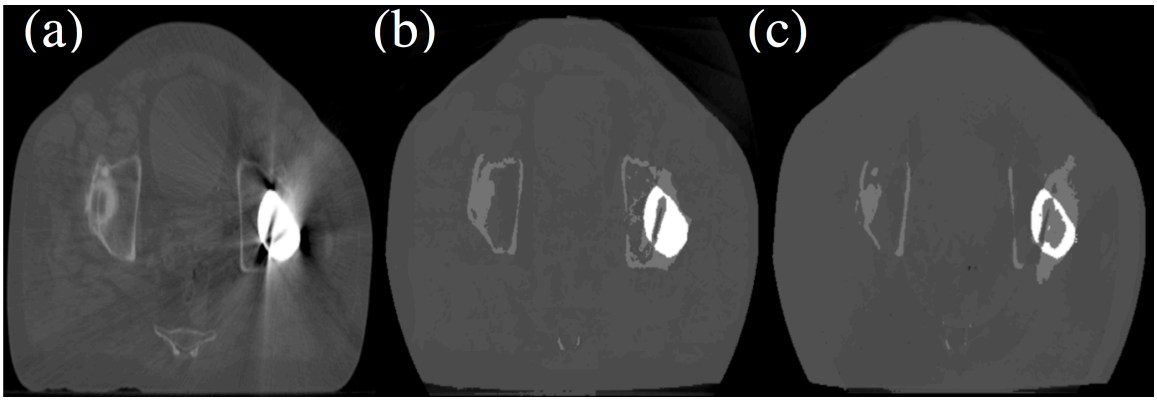

Figure 4: A slice of the pCT (a) and the resultant images after segmentation CBCT using the manual MLT ($sCBCT_{man}$) and the automated MLT ($sCBCT_{auto}$) (b and c respectively), showing the HU value difference in the left hip prosthesis.

301 Figure 5 shows the DVH of a prostate IMRT plan with a prescription dose of 70 Gy in
302 35 fractions. It shows the dose of the pCT, $sCBCT_{man}$ and $sCBCT_{auto}$ plans to the PTV,
303 rectum and bladder using the CC algorithm. Both $sCBCT_{man}$ and $sCBCT_{auto}$ plans showed
304 almost the same difference from the pCT plan, except for the PTV where $sCBCT_{man}$
305 showed better agreement, the difference in D_{max} between the pCT and $sCBCT_{man}$ plans
306 was –0.56%, and $sCBCT_{auto}$ was –1.4%. Compared with the pCT plan, the $sCBCT_{man}$ plan
307 underestimated D_{mean} and D_{min} by –1% and –0.3%, respectively, while the $sCBCT_{auto}$ plan
308 underestimated D_{mean} and D_{mean} by –1.6% and –1%, respectively. The MC and PB
309 algorithm showed similar results to CC algorithm (see Table 1 in the Appendix 1).
310 Compared with pCT plan, the bladder V65 was reduced by 56% and 58% in $sCBCT_{man}$
311 and $sCBCT_{auto}$ plans, respectively, when using CC algorithm, showing better bladder
312 sparing (Table 1). There was a tradeoff in the D95 of the PTV, which reduced by 9% and

14% in $sCBCT_{man}$ and $sCBCT_{auto}$ plans, respectively, when using the CC algorithm. Significant organ deformation was observed between the pCT and CBCT scans, especially in the bladder volume (>15% reduction). This deformation resulted in large differences in D_{mean} for the bladder in both $sCBCT_{man}$ (–48.8%) and $sCBCT_{auto}$ (–49.2%).

Previous studies used either deformable electron density or deformable image registration (DIR) to improve the dose calculation accuracy and to correct the uncertainty from organ deformation (11, 14). For a standard prostate patient, the accuracy of dose calculation could be improved by 1-2% using these methods. Thor et al (2011) stated that the accuracy of DIR can be affected by bowel gas and artefacts from gold fiducial markers

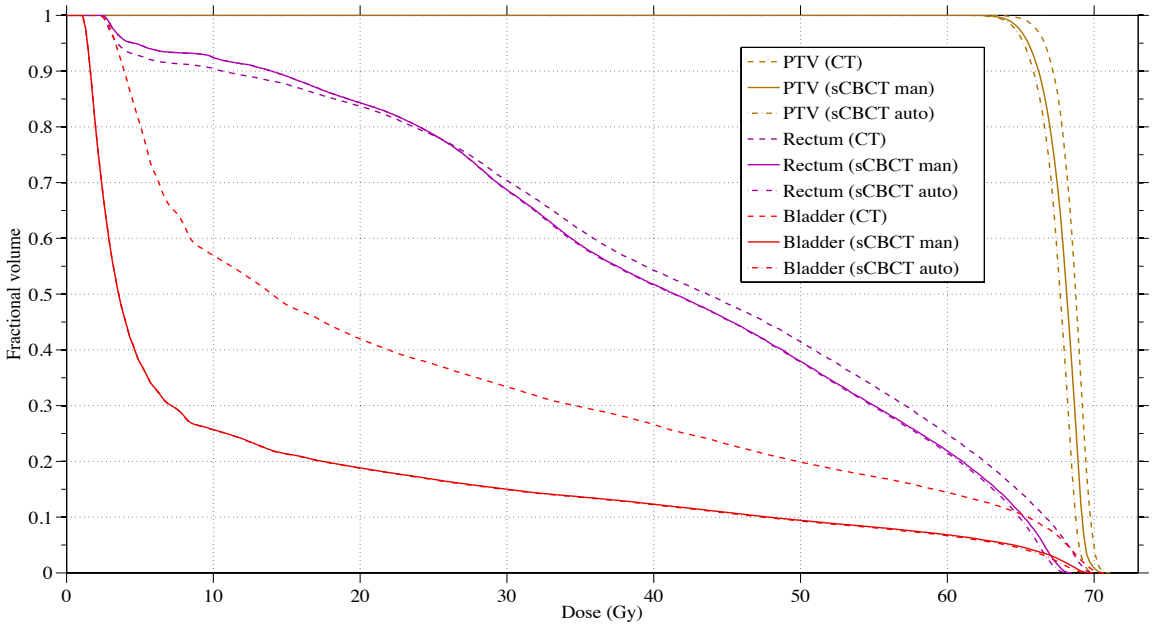

Figure 5: DVHs comparison pCT (–), $sCBCT_{man}$ (-) and $sCBCT_{auto}$ (-.) IMRT plans for PTV, rectum and bladder using CC algorithm.

inside the prostate (23). Thus, in some cases, DIR would result in no improvement in the accuracy of the dose calculation (14). In this study, the image quality of both pCT and sCBCT images was affected by streak artefacts caused by the presence of the bilateral hip

prostheses, thus the uncertainty associated with using DIR would be increased.

Table 1: PTV coverage for the pCT, $sCBCT_{man}$ and $sCBCT_{auto}$. The dose to 95% of PTV volume and minimum dose and the percentage of rectal and bladder volumes receiving 65 Gy and 70 Gy.

Scan		PTV		Rectum		Bladder	
		D95	Dmin	V65	V70	V65	V70
CT	PB	68.1	64.9	17.4	0.93	11.4	3.38
	CC	66.6	61.9	14.36	0	10.57	0.35
	MC	64.7	55.9	13.78	0	7	0
sCBCTman	PB	66.4	62.5	12.83	0	5.13	0.52
	CC	65.5	61.7	10.74	0	4.6	0
	MC	64.7	55.9	10.36	0	4.2	0
sCBCTauto	PB	66.2	62.1	12.25	0	4.96	0.3
	CC	65.2	61.3	9.66	0	4.39	0
	MC	64.5	53.5	9.26	0	4.01	0

Dunlop et al (2015) eliminated the need for, and uncertainties associated with, DIR by acquiring pCT on the same day as the CBCT, to be used as the ground truth for dose calculation (9). Thus additional doses could be delivered to the patients.

Figure 6(a) shows the CI values of the pCT, $sCBCT_{man}$ and $sCBCT_{auto}$ plans using PB, CC and MC algorithms. In general, the differences in the CI values between pCT and $sCBCT_{man}$ were smaller than those between pCT and $sCBCT_{auto}$ using all algorithms. The difference of the CI values between pCT and $sCBCT_{man}$ were –26.7 %, –42.8% and –15.6% when using PB, CC and MC algorithms, respectively. On the other hand, the difference of the CI values between pCT and $sCBCT_{auto}$ were –38.9%, –74.1% and –46.9% when using PB, CC and MC algorithms, respectively. However, according to the RTOG guidelines, the CI values between 0.9 and 1 indicate that the target volume is not adequately covered by the prescribed isodose with a minor violation, whereas CI values of less than

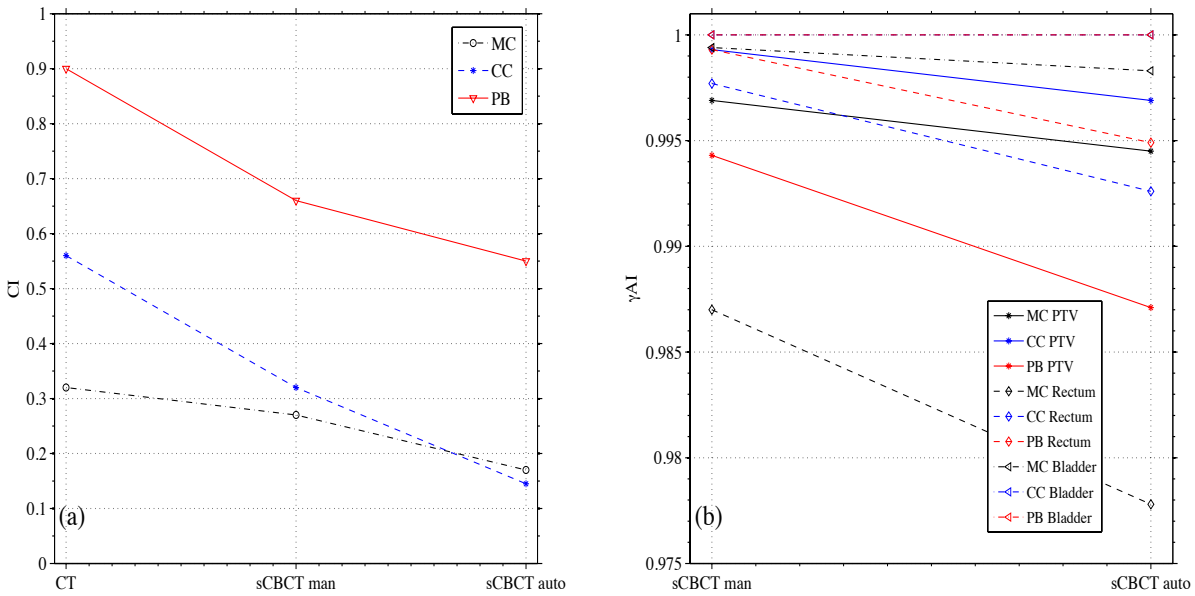

Figure 6: (a) Conformity index (CI) comparison between pCT, sCBCT$_{man}$ and sCBCT$_{auto}$ plans using PB, CC and MC algorithms. (b) Summary of the γ index with fixed DTA = 3 mm and DD = 3% for the calculation points falling inside the PTV, rectum and bladder, showing the fraction of points resulting with $\gamma < 1$.

0.9 the treatment plan are rated major violations but may nevertheless be considered to be acceptable (24, 25).

Figure 6(b) shows the γ agreement index (γAI) for the calculation points falling inside the PTV, rectum and bladder for the pCT, sCBCT$_{man}$ and sCBCT$_{auto}$ plans, showing the fraction of points resulting in $\gamma < 1$. For the bladder region, all the calculation points passed the gamma test when using the PB and CC algorithm, while using the MC algorithm, 99.9% and 99.8% showed $\gamma < 1$ for sCBCT$_{man}$ and sCBCT$_{auto}$, respectively. The lowest number of points that passed was found in the rectum region when using MC algorithm, where 98.7% showed $\gamma < 1$ in sCBCT$_{man}$ and 97.7% showed $\gamma < 1$ in sCBCT$_{auto}$ plans, which is clinically acceptable. Son et al stated that γ value is considered acceptable when the passing rate is greater than 95% with 3 mm DTA and 3% DD criteria (26).

Table 2: Dose comparison between pCT, $sCBCT_{man}$ and $sCBCT_{auto}$ plans at the isocentre using PB, CC and MC algorithms.

Scan	$sCBCT_{man}$			$sCBCT_{auto}$		
	PB	**CC**	**MC**	**PB**	**CC**	**MC**
Dose difference (%)	–0.81	–0.46	–0.39	–1.44	–1.36	–1.39

Table 2 shows the dose difference between pCT and sCBCT plans at the isocentre using all algorithms. In general, both $sCBCT_{man}$ and $sCBCT_{auto}$ plans showed differences of less than –2% compared with the pCT plan using all algorithms, which are both considered to be clinically acceptable. It can be seen that the difference between the $sCBCT_{man}$ and $sCBCT_{auto}$ is larger when using CC and MC algorithms than that when using the PB algorithm. This is due to the fact that the PB algorithm in OMP calculates dose to water while, the CC algorithm calculates dose to medium, as does the MC algorithm (27). Therefore, the PB algorithm would be less sensitive than CC and MC for calculating the dose using different scans. Thus MC and CC algorithms minimised uncertainty related to the dose calculation as well as identifying those introduced by different scans. However, for the MC calculation, the difference increased from –0.4% in the $sCBCT_{man}$ plan to –1.4% in $sCBCT_{auto}$ plan when compared with the pCT plan. On the other hand, the operator time required for defining the threshold values for different regions in $sCBCT_{man}$ was 8 hours while in $sCBCT_{auto}$, the threshold values were defined automatically and takes 20 min operator time. Some manual modification to ensure an appropriate assignment of each material in $sCBCT_{auto}$ scan was still needed to improve the accuracy but it requires much less (approximately 95%) operator time compared with $sCBCT_{man}$ scan. Dividing CBCT images into five concentric rings was accurate enough to correct the variation in the pixel

value with position in the CBCT images. As a result, the automated MLT algorithm reduced the operator time with an acceptable accuracy. This time saved could turn this technique from a research-based to a clinical implementation and makes it superior compared with the manual approach. Compared with the proposed technique in this paper, acquiring a new pCT is more time consuming, increase work load on physicists, physicians, and radiographers, which can take up to a day in a busy radiotherapy department, and more importantly additional dose is delivered to the patient.

4 Conclusion

The segmentation of CBCT images using methods in this study can be used for dose calculation. For a prostate patient with bilateral hip prostheses, the MLT algorithms achieved a sufficient dose calculation accuracy that is clinically acceptable. The automated MLT algorithm reduced the operator time associated with the MLT algorithm, making it possible to implement the technique into clinic. Thus this method would be feasible for ART, as an alternative to obtaining a new planning CT and re-outlining the structures. This method can be applicable for dose calculation on MR images and could be of interest to MR-based ART.

Reference

1. Langen KM, Jones DTL. Organ motion and its management. International Journal of Radiation Oncology* Biology* Physics. 2001;50(1):265-78
2. Ciernik IF, Baumert BG, Egli P, Glanzmann C, Ltolf UM. On-line correction of

beam portals in the treatment of prostate cancer using an endorectal balloon device. Radiotherapy and oncology. 2002;65(1):39-45.

3. Jaffray DA, Siewerdsen JH, Wong JW, Martinez AA. Flat-panel cone-beam computed to- mography for image-guided radiation therapy. International Journal of Radiation Oncology* Biology* Physics. 2002;53(5):1337-49.

4. Srinivasan K, Mohammadi M, Shepherd J. Cone beam computed tomography for adaptive radiotherapy treatment planning. Journal of Medical and Biological Engineering. 2014;34(4):377- 85.

5. Stock M, Pasler M, Birkfellner W, Homolka P, Poetter R, Georg D. Image quality and stability of image-guided radiotherapy (IGRT) devices: A comparative study. Radiotherapy and Oncology. 2009;93(1):1-7.

6. Fotina I, Hopfgartner J, Stock M, Steininger T, Ltgendorf-Caucig C, Georg D. Feasibility of CBCT-based dose calculation: comparative analysis of HU adjustment techniques. Radiotherapy and Oncology. 2012;104(2):249-56.

7. Richter A, Hu Q, Steglich D, Baier K, Wilbert J, Guckenberger M, et al. Investigation of the usability of conebeam CT data sets for dose calculation. Radiat Oncol. 2008;3(1):42.

8. Poludniowski GG, Evans PM, Webb S. Cone beam computed tomography number errors and consequences for radiotherapy planning: an investigation of correction methods. International Journal of Radiation Oncology* Biology* Physics. 2012;84(1):e109-e14.

9. Dunlop A, McQuaid D, Nill S, Murray J, Poludniowski G, Hansen VN, et al. Comparison of CT number calibration techniques for CBCT-based dose

calculation. Strahlentherapie und Onkologie. 2015;191(12):970-8.

10. van Zijtveld M, Dirkx M, Heijmen B. Correction of conebeam CT values using a planning CT for derivation of the dose of the day. Radiotherapy and Oncology. 2007;85(2):195-200.

11. Yang Y, Schreibmann E, Li T, Wang C, Xing L. Evaluation of on-board kV cone beam CT (CBCT)-based dose calculation. Physics in medicine and biology. 2007;52(3):685-705.

12. Boggula R, Lorenz F, Abo-Madyan Y, Lohr F, Wolff D, Boda-Heggemann J, et al. A new strategy for online adaptive prostate radiotherapy based on cone-beam CT. Zeitschrift fr Medizinische Physik. 2009;19(4):264-76.

13. Boggula R, Wertz H, Lorenz F, Madyan YA, Boda-Heggemann J, Schneider F, et al. A proposed strategy to implement CBCT images for replanning and dose calculations. International Journal of Radiation Oncology* Biology* Physics. 2007;69(3):S655-S6.

14. Onozato Y, Kadoya N, Fujita Y, Arai K, Dobashi S, Takeda K, et al. Evaluation of OnBoard kV Cone Beam Computed Tomography-Based Dose Calculation With Deformable Image Registration Using Hounsfield Unit Modifications. International Journal of Radiation Oncology* Biology* Physics. 2014;89(2):416-23.

15. Almatani T, Hugtenburg R, Lewis R, Barley S, Edwards M. Simplified material assignment for cone beam computed tomography-based dose calculations of prostate radiotherapy with hip prostheses. Journal of Radiotherapy in Practice. 2016;15(2):170-180.

16. Pineda AR, Siewerdsen JH, Tward DJ, editors. Analysis of image noise in 3D cone-

beam CT: Spatial and Fourier domain approaches under conditions of varying stationarity. Proc.SPIE 2008; 6913: 69131Q-69131Q-10.

17. Shaw CC. Cone beam computed tomography: Taylor & Francis; 2014.

18. Bourland JD. Image-guided Radiation Therapy: Crc Press; 2012.

19. Kawrakow I, Rogers DWO. The EGSnrc code system. NRC Report PIRS-701, NRC, Ottawa. 2000.

20. HPC Wales. Wales, UK. Available from: http://www.hpcwales.co.uk/. [Accessed 08 December 15] .

21. Deasy JO, Blanco AI, Clark VH. CERR: a computational environment for radiotherapy research. Medical physics. 2003;30(5):979-85.

22. ICRU. International Commission on Radiation Units and Measurements. Prescribing I. recording, and reporting photon-beam intensity-modulated radiation therapy (IMRT). ICRU Report 83. J icru. 2010;10:1-106.

23. Thor M, Petersen JBB, Bentzen L, Hyer M, Muren LP. Deformable image registration for contour propagation from CT to cone-beam CT scans in radiotherapy of prostate cancer. Acta Oncologica. 2011;50(6):918-25.

24. Feuvret L, Nol G, Mazeron J-J, Bey P. Conformity index: a review. International Journal of Radiation Oncology* Biology* Physics. 2006;64(2):333-42.

25. Petkovska S, Tolevska C, Kraleva S, Petreska E, editors. Conformity index for brain cancer patients. Conference on medical physics and biomedical engineering; 2010.

26. Son J, Baek T, Lee B, Shin D, Park SY, Park J, et al. A comparison of the quality assurance of four dosimetric tools for intensity modulated radiation therapy. Radiology and oncology. 2015;49(3):307-13.

27. Knöös T, Wieslander E, Cozzi L, Brink C, Fogliata A, Albers D, et al. Comparison of dose calculation algorithms for treatment planning in external photon beam therapy for clinical situations. Physics in medicine and biology. 2006;51(22):5785.

List of Figures

1. A slice of the pCT (a) and the original CBCT (b) and the resultant images after segmentation CBCT using the manual MLT ($sCBCT_{man}$) and the automated MLT($sCBCT_{auto}$). …….. 9

2. Comparison of the dose profile of pCT, $sCBCT_{man}$ and $sCBCT_{auto}$ plans at the isocentre depth using MC algorithm. The second y axis represents the $sCBCT_{man}$

number, $sCBCT_{auto}$ number and CT number. …….. 12

3. Right/Left hip and bone volume differences between pCT and $sCBCT_{man}$/$sCBCT_{auto}$. …… 13

4. A slice of the pCT (a) and the resultant images after segmentation CBCT using the manual MLT ($sCBCT_{man}$) and the automated MLT ($sCBCT_{auto}$) (b and c respectively), showing the HU value difference in the left hip prosthesis. …... 14

5. DVHs comparison pCT (–), $sCBCT_{man}$ (-) and $sCBCT_{auto}$ (-.) IMRT plans for PTV, rectum and bladder using CC algorithm. 15

6. (a) Conformity index (CI) comparison between pCT, $sCBCT_{man}$ and $sCBCT_{auto}$ plans using PB, CC and MC algorithm. (b) Summary of the γ index with fixed DTA = 3 mm and DD = 3% for the calculation points falling inside the PTV, rectum and bladder, showing the fraction of points resulting with $\gamma < 1$. …….. 16

7. Dose comparison between pCT, $sCBCT_{man}$ and $sCBCT_{auto}$ plans at the isocentre using PB, CC and MC algorithms. …….. 17